Geomechanics and Engineering, *Vol. 42, No. 1 (2025) 43-55*
https://doi.org/10.12989/gae.2025.42.1.043

Discrepancies of LiDAR registrations to capture potential displacements of mechanically stabilized earth walls

Gustavo O. Maldonado*, Marcel M. Maghiar[a],
Soonkie Nam[b], Md. Mehrab Hossain[c] and Shakil Ahmed[d]

Department or Civil Engineering & Construction, Georgia Southern University, Statesboro, GA 30460, USA

(*Received December7, 2024, Revised April 25, 2025, Accepted June 23, 2025*)

Abstract. This study considers terrestrial LiDAR to potentially capture undesirable displacements in mechanically stabilized earth walls (MSEWs), over time. In the USA, MSEWs have been used for almost 50 years and are becoming ubiquitous in bridge abutments. Time brings deterioration and the need to design and employ adequate inspection protocols for monitoring the integrity and deterioration rate of these structures. In that regard, the authors are closely working with the Georgia Department of Transportation (GDOT), USA. The current work aims to compare two scan-registration (scan-stitching) techniques to determine their relative accuracy. They are the target-based (TB) and the visual-aligned (VA) approaches. The relative spatial accuracy of their resulting virtual, 3D, point-cloud models, were compared against measurements completed in the field via a slow robotic total-station (RTS) instrument, with one-second angular accuracy, serving as the benchmarking device. The main goal of this study is to determine the minimum amplitudes of wall displacements that could be captured by the TB and VA approaches. The resulting georeferenced models showed that both techniques, TB and VA, presented almost the same accuracy when modeling MSEWs covering relatively small areas (0.23 and 0.38 ha). In a root-mean-square sense, the measurements obtained from the first analyzed bridge could capture most wall displacements larger than ~24 mm. Similarly, for the second bridge, both approaches could capture most wall displacements larger than ~11 mm. An additional multi-user analysis was completed to estimate the variability of the results due to users having different levels of experience with these techniques.

Keywords: displacements; LiDAR; MSE walls; settlements; target-based and visual-aligned registrations

1. Introduction

1.1 General background

Mechanically stabilized earth walls use resistance between backfill materials and reinforcing strips to retain embankments. The strips act as anchoring appendages of the different concrete elements forming the wall facing. The reinforcement varies but commonly include steel and geosynthetics. Due to their economy and stability, these walls have become ubiquitous in bridge abutments and other retaining structures. MSEWs were first introduced in the USA in 1972 (Mitchell and Villet 1987) and numerous are now constructed every year. Their design methods are well documented by the Federal Highway Administration, USA (Berg *et al*. 2009a, b). Those documents include general guidelines on performance monitoring but do not consider the latest available technologies. Nevertheless, recently, researchers have been incorporating new techniques to detect displacements in retaining walls. For example, Ko *et al*. (2021) conducted a small-scale experiment involving wall collapse and captured surface deformation and displacement using a 3D, image-based, digital-image correlation approach; Becker *et al*. (2024) employed terrestrial laser scanning to detect changes in soil surfaces leading to landslides; Wand *et al*. (2023) used 2D model tests to study the influence of tunneling on the earth pressure and ground settlement; and Lim *et al*. (2023) employed 2D finite element models to analyze settlements of the backfills and walls affected by groundwater drawdown. However, each of those works focused on particular conditions affecting their considered walls. A study by Tarawneh and Siddiqi (2014), which examined 339 MSEWs in Ohio, revealed that different problems may affect MSEWs, with as many as 95% of the walls suffering from either cosmetic or structural problems. As these structures age, their chance of deterioration arises, and the severity of their problems increases. The Georgia Department of Transportation (GDOT) employs these walls in numerous of its bridges and needs to investigate their aging problems during their life span and maintenance period, so proper inspection protocols can be generated. Our team works closely with GDOT on this issue.

Currently, there are no national or state level guidelines on when, what, and how to inspect retaining walls, while all bridges greater than 20 ft long are required to be inspected every two years as per the National Bridge Inspection Standards (Federal Highway Administration, USA, 2022). Instead, a problem-led approach to maintenance and repair

*Corresponding author, Professor
E-mail: gmaldonado@georgiasouthern.edu
[a]Ph.D.
[b]Ph.D.
[c]M.S. Student
[d]M.S. Student

ISSN: 2005-307X (Print), 2092-6219 (Online)

is usually applied, based on the results of visual inspections of the retaining walls. However, this approach can miss opportunities to economically extend the life of the retaining walls. By exploring and potentially adopting novel methods based on nondestructive (NDE) and noncontact evaluation technologies, problems could be detected more easily, quickly, and reliably than only using typical visual inspections.

A preliminary literature review revealed very little work done on developing inspection protocols and techniques for MSEWs and modular block walls (MBWs). Most of the studies on inspection guidelines focused on the construction stages and were not appropriate for preventive/maintenance purposes. In addition, the inspection methods were mostly based on visual inspections. Vankavelarr and Leshchinsky (2003) conducted a study of inspection guidelines for MSEWs, but their primary focus was on the construction stages, and they did not suggest a grading system. Sun and Graves (2013) reviewed the MSEWs inspection guidelines for bridge abutments, collecting inputs from 39 states in the United States and 2 provinces in Canada. They reported that only two states/provinces have maintenance handbooks for inspectors, although several states do examine the abutment walls during their regular bridge inspections. Only the state of Nebraska appears to have set up any kind of retaining wall inspection system (Jensen 2009) which is still based on the engineer's visual inspection. Wisconsin DOT also covers MSEW and MBWs inspections, under the heading of bridge ancillary structures, in their structural inspection manual, which does not consider the unique features of the reinforced earth walls (Wisconsin DOT, 2017). GDOT began evaluating MSEWs in 1979 and has devoted some effort to monitoring possible corrosion issues (Transportation Research Board 2012), but no other reports on the MSEW maintenance inspection guidelines were found in the preliminary literature review. Studies utilizing unmanned aerial vehicles (UAV) and photogrammetry have been supported by GDOT, but these focused solely on the analysis of ground images and topographic information. It is obvious that the capability of the technologies has been proven in different fields, but they have not been applied and verified for the retaining walls yet. Recently, Loosli (2025) indicated the differences, accuracies, and benefits of employing close-range photogrammetry (CRP) and airborne Light Detection and Ranging (LiDAR). These two techniques are comparable in horizontal accuracy, with UAV-based LiDAR presenting higher vertical accuracy and becoming more adequate for precise measurements. CRP is well suited for capturing detailed surface textures and visual appearances. Additionally, the terrestrial, static version of LiDAR (T-LiDAR) is even more accurate than its airborne type but requires multiple scanning positions to cover large areas.

Since the spatial areas covered in this work are relatively small, and accuracy is essential to capture small wall displacements, this study focuses on T-LiDAR techniques as non-destructive, non-contact means to detect undesirable, displacements in deteriorating MSEWs. In this regard, the use of the Leica Geosystems' ScanStation C10 laser scanner was investigated in this study. Its main characteristics are presented in the *Instrument*s section of this article. It was employed to generate virtual, 3D, point-cloud models that capture the existing spatial configurations of selected MSEWs. The idea is to fully scan a given MSEW at different times, generate similar 3D models at each time, and compare them for potential detection of wall displacements between those modelling events. In this regard, the relative accuracy of two different scan-stitching (scan-registration) techniques are investigated. They are described in the following subsection.

1.2 Scan-registration techniques

Individual laser-based scans are to be stitched together to form a full point-cloud model of a selected area. In general, each scan uses its own system of reference. Therefore, stitching them together consists in registering them into the same coordinate system. It is common to refer to that stitching process as a registration procedure. In this regard, there are two common registration techniques:

(1) The TB scheme employs a minimum of three common points (referred to as target points) to register two, or more, scans into the same system of coordinates, at once. There are different types of targets. Examples of them are 6-inch diameter, flat disks, with alternating quadrants, painted in black-&-white, and white spheres of different sizes (e.g., 6-inch or 9-inch diameter). This TB scheme is accurate but requires considerable time in the field to assure that enough targets are captured, at high resolution, by each scan to properly stitch all of them. Nevertheless, its associated registration work is accomplished by a computer algorithm in a relatively very short time. Several source of errors may affect the location of the corresponding targets when captured by different scans. After simultaneously stitching all scans, the quality of the attained registration can be estimated by observing the mean absolute error (MAE) and root mean square error (RMSE) of the final locations of the superposed target points.

(2) The other common registration technique is the cloud-to-cloud (CC) approach. It registers only two scans at a time and is characterized by its fast field operation. This is because it does not require various target points as the TB approach. However, the CC technique presents a slow registration process, requiring more labour. It consists of identifying a minimum of three common points on the two scans that are to be registered together. However, often those points are not necessarily at the same exact spatial location, but close to each other. This introduces and error that can later be minimized via software. Once two scans have been stitched, a third can be added to the initial two ones. Then, a fourth scan will be stitched and so on. Fortunately, Leica Geosystems has introduced an improved version of this technique, the VA process. It entails the manual aligning of a pair of scans on a horizontal plane (a plan view) and on a vertical plane (a side view). After the user completes the initial visual alignment of two scans, the software refines the stitching by maximizing the number of coincident points and minimizing the distance between quasi-coincident points. After stitching two scans, the quality of the corresponding registration can be estimated

by observing the attained quantity of overlapping points and the magnitude of the mean square error resulting from the quasi-coincident points

Since the VA approach does not require the acquisition of common targets to stitch scans together, it involves less time in the field than the TB technique. That is, operators following the TB approach need, approximately, 10 field minutes to acquire a single target and will have to do that three or more times (perhaps six times) per scanning station, substantially increasing their time in the field. Conversely, when registering the scans in a computer laboratory, the TB scheme is very fast, as it is done automatically and almost instantaneously by the software algorithm. In this task, the VA approach is rather slow and time consuming. It involves manual intervention to register one scan at a time, substantially increasing laboratory time. Since work on the field is more unpredictable, due to weather conditions, some operators may prefer to quickly complete the field tasks and spend more time in a computer laboratory, if accuracy is not compromised.

1.3 Objective

The magnitude of the wall displacements that can be captured via laser scanning depends on the accuracy attained in their resulting point-cloud models. This leads to the main objective of this work which is to determine the relative accuracy of the resulting virtual, 3D, point-cloud models of MSEWs, in highway bridges, generated via the TB and VA registration approaches. Their relative accuracy is established against classical field measurements completed with an accurate, one-second, robotic total station (RTS) instrument, Leica Geosystems' TCRP 1201+ R1000. In this work, this device serves as the benchmark instrument. Its main characteristics are presented in the *Instruments* section of this article. It only acquires the position of one point at a time, versus the 50,000-1,000,000 points per second captured by modern laser scanners.

The TB and VA registration procedures were selected to be compared because differences in their relative accuracies have already been reported in a previous project with different characteristics, as described in the following subsection.

1.4 Previous work

A previous study by Maldonado *et al*. (2024) analyzed the resulting relative spatial accuracy of the TB and VA registrations techniques. They were applied to sets of scans completed by the same scanning device, ScanStation C10. That work considered 45 checkpoints to analyze the relative accuracy of the resulting point-cloud models with respect to an accurate 3-sec RTS instrument, Topcon PS-103A. From the final georeferenced TB and VA models, 45 point positions and 995 non-repeated distances, among the 45 points, were extracted and compared against the same positions and distances completed in the field with the RTS instrument. First, that work involved 21 scans, but after performing the VA approach, it resulted in large errors (~15 cm). To increase their overlapping and improve accuracy,

Fig. 1 Locations (red dots) of the 34 scans completed for the Herald Plaza Project, along a closed loop

(a) Targets T2 and T3 as seen in a plan view, from a distance

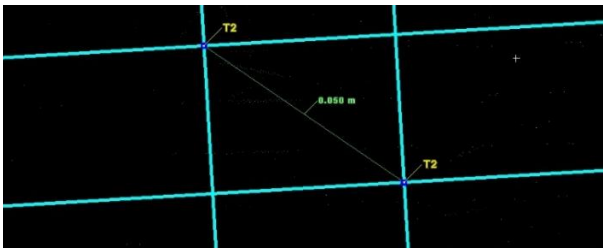

(b) Non-merged [NM] common targets T2, as seen zoomed in.

Fig. 2 Targets as observed in the G-VA LiDAR [NM] model of Herald Plaza

13 more scans were added. That is, a total of 34 full scans were involved to model Herald Plaza, a 1.4-hectarea, commercial area in Statesboro, GA. As shown in Fig. 1, the relative location of those 34 scans followed a closed path, with spatial superposition occurring only between a few close neighboring scans. The added scans reduced the errors to ~5 cm, as seen in Fig. 2(b). The total length of the closed main loop was approximately 360 m. The final average distances separating neighboring scans were ~15 m, ranging from ~4 m to ~27 m.

Table 1 shows the statistics of spatial discrepancies corresponding to that work. It involved the comparison of point positions and distances, extracted from the resulting G-TB LiDAR model (where G stands for georeferenced), against measurements, completed in the field, with the indicated RTS instrument. Similarly, the same table shows those discrepancies between the resulting G-VA LiDAR model and the same RTS instrument. It should be mentioned that even though the georeferencing registration of that VA model was successfully completed, their potentially coincident ground control points (GCPs) were not merged [NM] into a single point. That is, in the

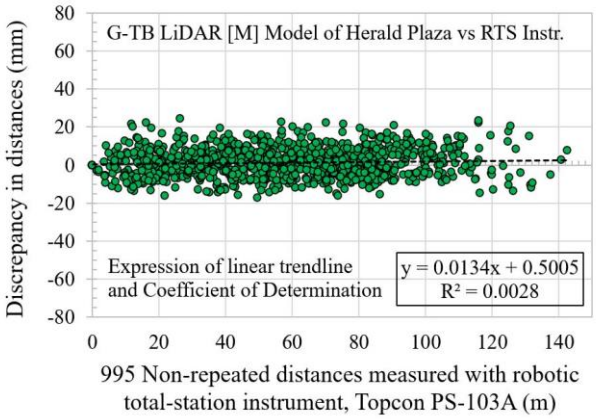

Fig. 3 Distance discrepancies – G-TB LiDAR [M] model of Herald Plaza vs RTS (Topcon PS-103A)

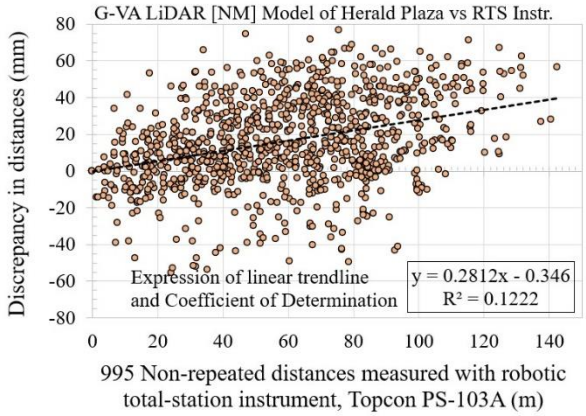

Fig. 4 Distance discrepancies – G-VA LiDAR [NM] model of Herald Plaza vs RTS (Topcon PS-103A)

Table 1 Discrepancies attained by Maldonado *et al*. (2024) in Point-Cloud Models of Herald Plaza, with respect to measurements via an RTS instrument (Topcon PS-103A)

Statistical Function	G-TB LiDAR [M]*[1] vs RTS Instrument		G-VA LiDAR [NM]*[2] vs RTS Instrument	
	Position Abs. Discr. (mm)	Distance Discr. (mm)	Position Abs. Discr. (mm)	Distance Discr. (mm)
Max	15.5	24.3	59.0	76.6
Min	2.5	-17.2	2.2	-55.7
Mean	= MAE	1.3	= MAE	16.2
MAE	8.9	6.2	27.0	22.9
Median	= Median (Abs)	1.1	= Median (Abs)	14.5
Median (Abs)	8.5	5.4	28.9	18.0
STD-P*[3]	3.3	7.6	13.8	23.9
STD-S*[4]	3.3	7.6	13.9	23.9
RMSE	9.5	7.7	30.3	28.8

*[1][M]: with merged GCPs. *[2][NM]: with non-merged GCPs. *[3]STD-P: standard deviation of the population. *[4]STD-S: standard deviation of the sample

resulting G-VA point-cloud, several of the same GCPs were observed in very close proximity to each other, but not exactly at the same location. This can be observed in Fig. 2, where target T2 is shown at two different locations, separated by 50 mm.

The non-merged targets were contributing to the larger discrepancies attained in the G-VA model versus those observed in the G-TB model. That work analyzed the relative position accuracy of 45 points and 995 non-repeated distances among them. With permission from the authors, their results are reproduced here in metric units, and shown in Tables 1 and 2, and Figs. 3 and 4.

Figs. 3 and 4 show, respectively, the discrepancies in 995 non-repeated distances, extracted from the G-TB LiDAR [M] and G-VA LiDAR [NM] models of Herald Plaza, and compared against the same 995 distances measured with an accurate RTS instrument, Topcon PS-103A.

The current work reduced the larger errors shown in Table 1 and Fig. 4 for the G-VA LiDAR [NM] model of Herald Plaza. This was accomplished by merging the targets in the final G-VA model. For this, a new point-cloud model was generated by adjusting two registration parameters in the Leica Cyclone Core software: (i) the *Auto-Add Constraint Tolerance* was set at 9 mm, and (ii) the *Default Max Search Distance* was set at 0.2 m. The option *Merge Targets when Freezing* was left at its default YES value. This resulted in a VA point cloud with merged GCPs. Because of this, in Table 2, the new G-VA model is referred to as G-VA LiDAR [M]. It compares the discrepancies of this new model against measurements, obtained in the field, with the Topcon PS-103A total-station instrument. Fig. 5 shows the discrepancies in distances extracted from the new G-VA LiDAR [M] model versus the same distances measured, in the field, with RTS Topcon PS-103A.

When comparing the older G-VA LiDAR [NM] model, in Table 1 and Fig. 4, against the new G-VA LiDAR [M] model, with merged GCPs, in Table 2 and Fig. 5, it is observed that 45 position discrepancies reduced their RMSE from 30.3 mm to 16.7 mm (a 45% reduction) and the RMSE for 995 distance discrepancies decreased from 29.8 mm to 15.1 mm (a 48% reduction).

Table 2 Discrepancies attained in the G-VA LiDAR [M] model, with merged GCPs, of Herald Plaza, with respect to measurements via an RTS instrument (Topcon PS-103A)

Statistical Function	G-VA LiDAR [M] vs RTS Instrument	
	Position Abs. Discrepancies (mm)	Distance Discrepancies (mm)
Max	35.7	47.9
Min	2.9	-23.5
Mean	= MAE	8.3
MAE	15.0	11.4
Median	= Median (Abs)	6.9
Median (Abs)	12.7	8.6
STD-P	7.4	12.6
STD-S	7.5	12.6
RMSE	16.7	15.1

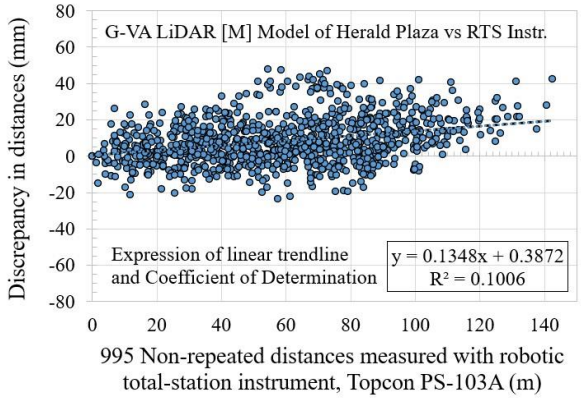

Fig. 5 Distance discrepancies – G-VA LiDAR [M] model of Herald Plaza vs RTS (Topcon PS-103A)

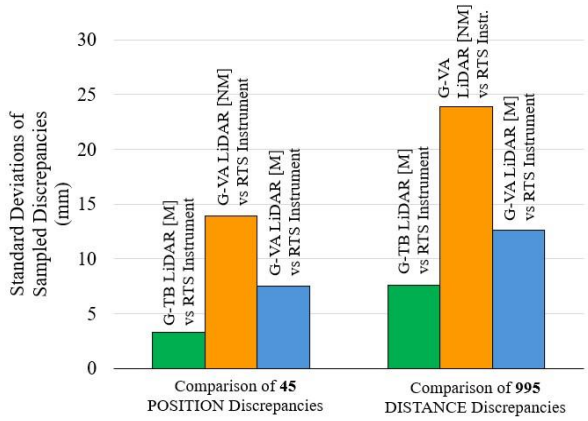

Fig. 6 Discrepancies in Herald Plaza. Each LiDAR model vs measurements via RTS, Topcon PS-103A

Fig. 6 presents a comparison between the LiDAR models of Herald Plaza. It shows the standard deviations of sampled discrepancies between each LiDAR model and measurements completed with the Topcon PS-103A robotic, total station. There, it is observed that the georeferenced VA model with non-merged GCPs presents the largest discrepancies with respect to the referred RTS instrument.

The resulting discrepancies indicate that the VA LiDAR model of Herald Plaza, with merged GCPs, is more accurate than the one with non-merged GCPs. Therefore, the current study on MSEWs only generated G-TB and G-VA LiDAR models with merged GCPs.

1.4 Sites considered in the current project

This study analyses the relative accuracies of virtual, 3D, point-cloud models (G-TB and G-VA) of MSEWs at 2 different highway bridges, in Southeast Georgia. Each bridge has two retaining walls, one at each of its 2 abutments. That is, a total of 4 MSEWs were analyzed.

The first bridge is at the intersection of Jimmy Deloach Parkway and Crossgate Road, in Port Wentworth, GA. The second bridge is at the intersection of highway I-16 and Old River Road, near Meldrim, GA. Respectively, these two bridges are herein referred to as 1-CG and 2-OR. Their plan views are presented in Fig. 7. The area involving bridge 1-CG is approximately 0.23 hectares whereas bridge 2-OR covers nearly 0.38 hectares.

(a) Bridge 1-CG, at the intersection of Jimmy Deloach Pkwy and Crossgate Rd, Port Wentworth, GA, USA

(b) Bridge 2-OR, at the intersection of I-16 and Old River Rd, near Meldrim, GA, USA

Fig. 7 MSEWs at the two bridges considered in this study. (Aerial views from Google Maps, Dec. 5, 2024)

The 2 MSEWs, at each bridge, required only 6 scans to generate the point clouds that captured their full wall facings. Each of those 6 scans presented substantial spatial superposition among all the other scans at the same bridge. As it was the case in the Herald Plaza project, the ScanStation C10 scanner was also employed for these 2 bridges. However, in this new study, a more accurate, one-second, RTS device, served as benchmark. The characteristics of these two instruments are presented the following section.

2. Instruments

Two different instruments were employed in this work. Their main characteristics are described in the following two paragraphs:

(1) The already referred RTS from Leica Geosystems, model *TCRP 1201+ R1000*. It performs laser-based distance measurements by determining the phase differences between the transmitted and reflected light. This is the most accurate device in this study and was considered the benchmark instrument. According to its manufacturer (Leica 2007) this device has a range of 1,500 m when used with a 360° reflector prism, under light haze with visibility of 20 km, or moderate sunlight with slight heat shimmer. Using a reflector and standard measuring mode, the standard deviation, σ, of its error, for distance d measurement, is σ=1 mm+1.5 ppm*d. On reflectorless

Table 3 Characteristics of both 6-sided traverses

Traverse at Bridge	Perimeter	Ang. Error of Closure	Longitudinal Precision	Elev. Error of Closure
	(m)	(sec)	(ratio)	(mm)
1-CG	358.858	56.0	1/86,406	-2.7
2-OR	212.683	-14.5	1/26,324	-7.9

mode, for distances d < 500 m, σ=2 mm+2 ppm*d, while for distances d > 500 m, σ=4 mm+2 ppm*d. Its vertical and horizontal angular accuracies are 1 arcsecond. This RTS instrument was used with a 360° reflector prism, Leica's GRZ4, while completing closed-traverse procedures to establish ground control points (GCPs) for georeferencing purposes. Additionally, it was used in reflectorless mode to acquire coordinates of selected checkpoints (CPs). In reflectorless mode, it can measure targets more than 1,000 m away.

(2) A terrestrial, laser-based scanner from Leica Geosystems, *ScanStation C10*. This device has a maximum scanning rate of 50,000 points per second and was employed to generate all 3D, point-cloud models of the selected walls in this study. According to Leica Geosystems (Leica 2014), this device has a position accuracy of σ = 6 mm and a measurement accuracy of σ = 4 mm, both at 1-50 m range. Its horizontal and vertical angular accuracies are 12 seconds. It has a 300-meter scanning range at 90% albedo and 134 m at 18% albedo. For proper verticalization, this instrument has a dual-axis compensator with a 1.5-sec accuracy.

3. Methodology

The same methodology was implemented for each of the two considered bridges. It consisted of various sequential tasks, as described below.

3.1 Task 1 - Establishment of GCPs

In each bridge, a fixed frame of reference was selected to work with accurate and conveniently adopted local coordinates. For this purpose, 6 GCPs were established on the lower roadway, near and below each bridge. These points were materialized with steel nails and served as vertices of 6-sided, closed, polygonal traverses.

The RTS instrument was used for all angular and longitudinal traverse measurements. The resulting coordinates for the GCPs were determined by balancing errors of closure. Characteristics of those traverses, including their errors of closure and attained longitudinal precisions, are presented in Table 3. The longitudinal traverse errors were balanced using the popular Compass rule, also known as the Bowditch rule.

3.2 Task 2 - Laser scanning

This task consisted in collecting spatial data to later generate full, laser-based, 3D, point-cloud models of both MSEWs at each bridge. This was accomplished by using the C10 scanner at 6 different scanning stations per bridge. That is, 3 scans were performed near each retaining wall. In all cases, scans covered a full horizontal angle of 360° at medium resolution. In the C10 scanner, this resolution level captures the positions of points separated by 1 cm when they are located at 10 m from the scanner. During this activity, a spherical target was located on each GCP, and it was acquired by each scan. This target acquisition has a double purpose: (i) to have the option to use them for stitching the individual scans; and (ii) to employ them for georeferencing the full, 3D, point-cloud models into a common coordinate system.

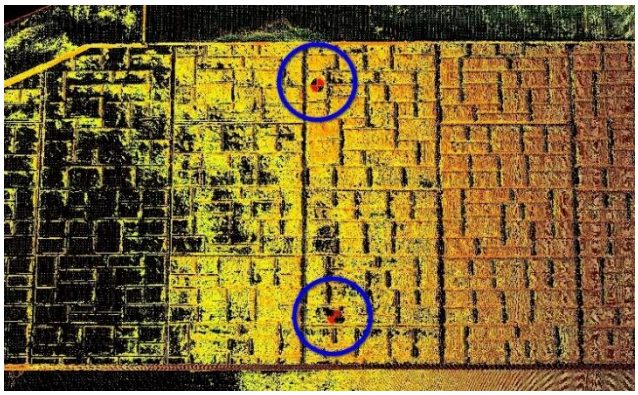

Fig. 8 Two painted checkpoints (CPs), as seen in a point-cloud, LiDAR model of one MSEW, at bridge 2-OR

3.3 Task 3 – Acquisition of CP Coordinates

To monitor potential displacements after a certain period (e.g., a few months or years), 6 CPs were marked on each MSEW. That is, 12 CPs were considered at each bridge. They consisted of 6-inch-diameter circles, with alternating black-&-white quadrants, painted on the MSEWs.

Those CPs were marked near the wings and on the central sections of each MSEW, with 3 of them near the top of the walls and 3 near their bottom sections. Fig. 8 shows two scanned CPs, inside blue circles. The RTS instrument was employed in the field to acquire the position coordinates of all 12 CPs per bridge. For this, the RTS device was stationed at one GCP and used a second GCP as backsight. Hence, the acquired coordinates of the CPs were in the same system of reference as the coordinates of those GCPs.

3.4 Task 4 – Noise cleaning

The 6 scans completed at each bridge were individually cleaned by removing undesired noise, i.e., vehicular or pedestrian traffic and solar beams. This cleaning was performed by using the Cyclone Core software. After cleaning each scan, they were properly saved to avoid the need to repeat the cleaning processes in subsequent tasks. This required to follow a proper procedure in the Cyclone Core software, involving the Model and Control spaces of each scan.

Table 4 Characteristics of the Target-Based Registrations

		Bridge 1-CG	Bridge 2-OR
Enabled Targets	Quantity	4	6
	Labels	TA, TB, TD, TE	TA, TB, TC, TD, TE, TF
Disabled Targets	Quantity	2	0
	Labels	TC, TF	Not Applicable
Number of Constraint Links (CLs)	Available	70	90
	Enabled	18	74
	Disabled	52	16
Mean Abs. Error	in Enabled CLs	< 1 mm	2 mm
	in Disabled CLs	2 mm	16 mm
Error Range	in Enabled CLs	< 1 mm	0-6 mm
	in Disabled CLs	1-9 mm	10-21 mm

3.5 Task 5 – Generation of target-based model

The point cloud captured by an individual scan has its own coordinate system of reference. This system differs from scan to scan. Therefore, it is necessary to register them into the same frame of reference. The registration occurs while stitching the scans to generate a full model. One technique to complete this process translates and rotates scans so common target points, in neighboring scans, coincide. However, this coincidence is not perfect and carries some small errors. This target-based approach is referred to as TB and is one of the two techniques considered in this work. The required minimum number of common targets to stitch two scans together is 3, or 2 for perfectly verticalized scanners. For this purpose, during field scanning, our team captured the same 6 common targets, TA, TB, TC, TD, TE, and TF, in all 6 scans at each bridge. Then, the registration process was performed in computer workstations at Georgia Southern's Built Environment and Modeling (BEaM) laboratory. It employed an optimization algorithm, based on least squares, implemented by Leica's Cyclone Core software package. During this stitching process, a single target, when captured by two scans, generates a spatial constraint link (CL), connecting those two scans. Three of those links are necessary to stitch (register) two scans together. However, due to unavoidable minor errors (e.g., slight mispositioning, or inaccurate verticalization of targets, or minor miscalibration of instruments, etc.), not all targets attain absolute coincidence. Even after applying the error minimization algorithm, each CL still carries a small error, which differs from link to link. Purposely, in this work, we employed 6 common targets in each scan, and this resulted in an abundantly redundant number of CLs. This redundancy allowed to discard links containing larger errors.

Table 4 shows the main characteristics and errors attained in the TB registrations for both bridges. In general, the TB approach requires extended field time to accurately capture several required targets per scan. On the other hand, the associated registration process is swift and automatically performed by the software, involving minimum post-processing time in the laboratory.

Table 5 Characteristics of the Visual-Aligned Registrations

	Bridge 1-CG		Bridge 2-OR	
Stitched Scans	RMSE* (mm)	Overlap Pt. Count ($\times 10^3$)	RMSE* (mm)	Overlap Pt. Count ($\times 10^3$)
1 & 2	13.1	790	9.6	1,027
2 & 3	10.7	928	8.5	833
3 & 4	14.4	1,116	13.5	507
4 & 5	14.6	972	10.8	1028
5 & 6	12.6	998	7.5	865
6 & 1	15.9	958	NA	NA

*RMSE: Root mean square error in quasi-coincident points

3.6 Task 6 – Generation of visual-aligned model

The alternative registration approach, considered in this study, is known as cloud-to-cloud (CC). It consists of manually selecting a few common points in 2 neighboring scans and then superposing them in the same manner that targets were superposed in the TB technique. However, usually, the selected common points are not exactly at the same spatial positions in the involved scans. Additionally, this scheme requires to stitch only two scans at a time, increasing the changes of error propagation in subsequent scans. Therefore, this technique may result in final models with increased inaccuracies.

Opportunely, Leica Geosystem's has improved the CC manual approach by allowing the user to approximately visual align two neighboring scans in a horizontal plan view and in a vertical side view. After this human-based alignment, Leica's software uses an optimization algorithm to refine it and maximize the number of nearly superposed points in both involved neighboring scans. This scheme is referred to as the visual-aligned (VA) registration technique. Since it does not require the use of stitching targets, it saves time in the field but involves more laboratory postprocessing time than the TB approach. Table 5 shows the main characteristics and errors attained in the VA registrations of both bridges.

3.7 Task 7 – Georeferencing of final models

Once the 2 resulting full, 3D, point-cloud models (TB and VA) for each bridge were finalized, they were georeferenced in the same local system of coordinates. This system is the same employed by the GCPs (i.e., the vertices of the closed traverses). After georeferencing the TB and VA models, they are referred to as G-TB and G-VA, respectively. This referencing process is necessary to later compare point positions and distances extracted from different LiDAR models or measured in the field via the RTS instrument.

The georeferencing work is relatively simple and involves the registration of the full models, TB and VA, into a point cloud containing only a few points. That is, at least 3

Table 6 Characteristics of the G-TB Registrations

		Bridge 1-CG	Bridge 2-OR
Enabled Targets at GCPs	Quantity	3	5
	Labels	TA, TD, TE	TA, TB, TC, TD, TE
Disabled Targets	Quantity	2	1
	Labels	TB, TF	TF
Number of Constraint Links (CLs)	Available	5	6
	Enabled	3	5
	Disabled	2	1
Mean Abs. Error	in Enabled CLs	2 mm	4 mm
	in Disabled CLs	7 mm	19 mm
Error Range	in Enabled CLs	2-3 mm	2-6 mm
	in Disabled CLs	6-8 mm	19 mm

Table 7 Characteristics of the G-VA Registrations

		Bridge 1-CG	Bridge 2-OR
Enabled Targets at GCPs	Quantity	4	5
	Labels	TA, TD, TE, TF	TA, TB, TC, TD, TE
Disabled Targets	Quantity	1	1
	Labels	TB	TF
Number of Constraint Links (CLs)	Available	5	6
	Enabled	4	5
	Disabled	1	1
Mean Abs. Error	in Enabled CLs	3 mm	4 mm
	in Disabled CLs	9 mm	19 mm
Error Range	in Enabled CLs	1-4 mm	2-7 mm
	in Disabled CLs	9 mm	19 mm

GCPs. This requires that the spatial locations of the involved GCPs are acquired while scanning in the field. Fort this, targets are positioned on those GCPs, and they are usually acquired by the scanning station that is closest to a particular target. They do not need to be acquired by all scans.

Tables 6 and 7 show the main characteristics and resulting errors, in both bridges, after completing the georeferencing registrations for their TB and VA models, respectively.

3.8 Task 8 – G-TB vs RTS and G-VA vs RTS

For each bridge, the locations of their 12 CPs were extracted from the finalized G-TB and G-VA models. These positions were compared against the same positions measured in the field via the accurate RTS instrument. Additionally, for each bridge, all possible 66 non-repeated distances among its 12 CPs were calculated to compare them against the same distances measured by the RTS device. The analysis of that comparison is presented in the Results section of this article.

Table 8 Relative error comparison, TB approach vs RTS, and VA approach vs RTS

Bridge (Area)	Comparison Type	Positions of 12 Checkpoints		Non-Repeated 66 Distances	
		MAE (mm)	RMSE (mm)	MAE (mm)	RMSE (mm)
1-CG (0.23 ha)	G-TB vs RTS	18.7	23.0	4.0	4.9
	G-VA vs RTS	16.0	20.6	2.8	3.6
2-OR (0.38 ha)	G-TB vs RTS	9.4	10.2	5.9	7.6
	G-VA vs RTS	7.0	7.4	3.7	4.8

4. Results

The obtained results assist in estimating the magnitude of potential undesirable displacements that MSEWs may undergo and could be captured by T-LiDAR models.

As previously mentioned, 12 CPs were marked on the 2 retaining walls at each bridge. That is, 6 CPs on each wall. This was done by painting, at their locations, 6-inch circles with alternating black-&-white quadrants. Later, for accuracy comparison purposes, the coordinates of those CPs were extracted from three different sources: (i) the final G-TB model, (ii) the final G-VA model, and (iii) field acquisition with the accurate RTS instrument, which is the benchmark instrument in this work. For improved accuracies, all generated LiDAR models contained merged [M] targets. Since this has been the case in all point-cloud models produced in this study, their names do not include the [M] designation.

After the coordinates of the CPs were extracted from each LiDAR model, they were compared against those captured by the RTS device. The 2 middle columns of Table 8 show the Mean Absolute Error (MAE) and Root Mean Square Error (RMSE) in 12 position discrepancies calculated by subtracting the positions measured, in the field, with the RTS instrument from the positions extracted from the finalized georeferenced LiDAR models, for each bridge.

Distance discrepancies were also analyzed for each bridge. For this, all 66 non-repeated distances, among all 12 CPs, were vectorially calculated for both LiDAR models of each bridge, and the same distances were determined using field coordinates acquired by the RTS benchmark device. That is, the distances extracted from the G-TB and G-VA models were compared against those determined by the RTS instrument. The last 2 columns of Table 8 present the MAE and RMSE values corresponding to distance discrepancies measured along those 66 lengths in each bridge.

Table 8 shows that bridge 1-CG presents larger position discrepancies than bridge 2-OR. However, 1-CG shows slightly less discrepancies in distances. For ready comparison, their MAE and RMSE ratios (bridge 1-CG / bridge 2-OR) are presented in Table 9.

The comparisons in Tables 8 and 9 assist in estimating the relative accuracy of the analyzed G-TB and G-VA models with respect to the RTS benchmark instrument. In point positions, the LiDAR models of bridge 1-CG presents

Table 9 MAE and RMSE ratios (bridge 1-CG/bridge 2-OR)

Considered Bridge Ratio	LiDAR Model	Positions of 12 Checkpoints		Non-Repeated 66 Distances	
		MAE Ratio	RMSE Ratio	MAE Ratio	RMSE Ratio
1-CG / 2-OR	G-TB	~2.0	~2.3	~0.7	~0.6
	G-VA	~2.3	~2.8	~0.8	~0.8

Table 10 Comparison of georeferenced LiDAR models, G-TB versus G-VA, in both bridges

Bridge	Ratio	Positions of 12 Checkpoints		Non-Repeated 66 Distances	
		MAE Ratio	RMSE Ratio	MAE Ratio	RMSE Ratio
1-CG	G-TB / G-VA	~1.2	~1.1	~1.4	~1.4
2-OR	G-TB / G-VA	~1.3	~1.4	~1.6	~1.6

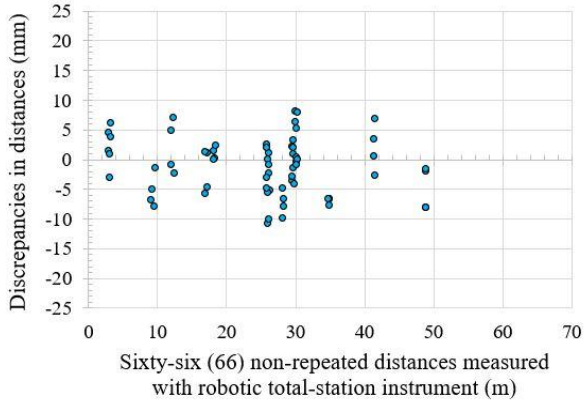

Fig. 9 Distance discrepancies, at Bridge 1-CG, between G-TB model and robotic total-station instrument

larger discrepancies (~2.0-2.8 times) with respect to the RTS device than the LiDAR models of bridge 2-OR. However, in distances, the discrepancies of the LiDAR models of bridge 1-CG present lower values (~0.6-0.8 times) than those of the LiDAR models of bridge 2-OR.

Additionally, Table 10 shows that, in both bridges, the G-VA models are slightly more accurate (~1.1-1.4 times in positions, and ~1.4-1.6 times in distances) than their G-TB models.

For bridge 1-CG, Fig. 9 presents the discrepancies in distances extracted from the G-TB model versus the same distances measured, in the field, with the RTS instrument.

Likewise, Fig. 10 presents distance discrepancies between the G-VA model and the RTS device. Similarly, for bridge 2-OR, Fig. 11 shows discrepancies in distances between its G-TB model and the RTS instrument. Similarly,

Fig. 12 shows discrepancies in distances between the G-VA model and the RTS device, for bridge 2-OR.

The extraction of CP coordinates from the final georeferenced, point-cloud models presents an extra source of uncertainty. This is because the exact position of a given CP may not have been hit/scanned by a laser beam. Nevertheless, there are several other scanned points very close to the location of that CP. Hence, in this study, the

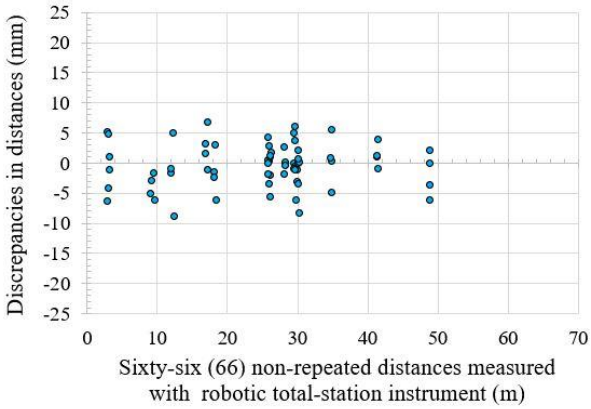

Fig. 10 Distance discrepancies, at Bridge 1-CG, between G-VA model and robotic total-station instrument

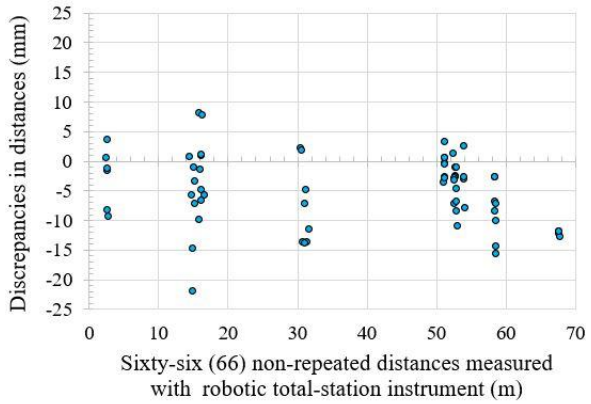

Fig. 11 Distance discrepancies at bridge 2-OR, between G-TB model and robotic total-station instrument

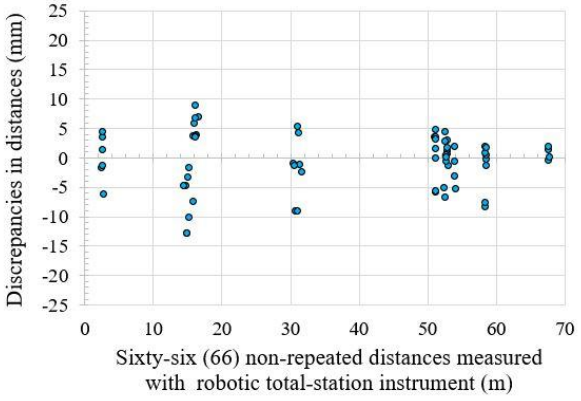

Fig. 12 Distance discrepancies, at Bridge 2-OR, between G-VA model and robotic total-station instrument

software users assigned to each CP the coordinates of the scanned point that they estimated the closest to that CP. Since different users may select different close by points, an additional error analysis was performed on bridge 2-OR, considering three more different users. That is, a total of four users, one from 2023 (U23a) and three from 2024 (U24a, U24b, & U24c), extracted the coordinates of all 12 CPs from the point clouds of that bridge.

Table 11 Characteristics of G-TB registrations for bridge 2-OR, by different users

Bridge 2-OR		G-TB Registrations by users	
		U23a	U24a, b, c
Enabled Targets	Quantity	5	3
	Labels	TA, TB, TC, TD, TE	TA, TB, TE
Disabled Targets	Quantity	1	3
	Labels	TF	TC, TD, TF
Number of Constraint Links (CLs)	Available	6	6
	Enabled	5	3
	Disabled	1	3
Mean Abs. Error	in Enabled CLs	4 mm	2 mm
	in Disabled CLs	19 mm	11 mm
Error Range	in Enabled CLs	2-6 mm	1-3 mm
	in Disabled CLs	19 mm	6-19 mm

Table 12 Characteristics of G-VA registrations for bridge 2-OR, by different users

Bridge 2-OR		G-VA Registrations by users	
		U23a	U24a, b, c
Enabled Targets	Quantity	5	3
	Labels	TA, TB, TC, TD, TE	TA, TB, TE
Disabled Targets	Quantity	1	3
	Labels	TF	TC, TD, TF
Number of Constraint Links (CLs)	Available	6	6
	Enabled	5	3
	Disabled	1	3
Mean Abs. Error	in Enabled CLs	4 mm	2 mm
	in Disabled CLs	19 mm	11 mm
Error Range	in Enabled CLs	2-7 mm	1-3 mm
	in Disabled CLs	19 mm	6-20 mm

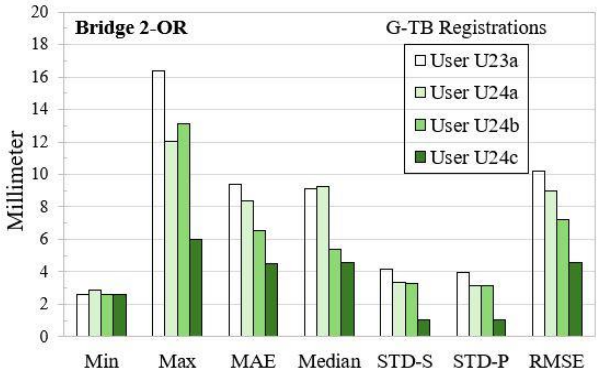

Fig. 13 4-user statistics of position discrepancies in 12 checkpoints – G-TB models vs RTS instrument

Users U24a, b, & c employed the same TB and VA registrations previously generated by U23a. The characteristics of those registrations were already shown in Tables 4 and 5, respectively. However, users U24a, b, & c generated their own, common, G-TB and G-VA registrations.

A comparison of the characteristics of the georeferenced registrations by U23a and by U24a, b, & c, is presented in Tables 11 and 12, respectively. The statistics for position discrepancies (with respect to measurements completed via the RTS instrument), in all 12 CPs, are presented in Fig. 13 for positions extracted from the G-TB model, and in Fig. 14 for positions extracted from the G-VA model. The averaged position statistics for all four users are shown on Fig. 15.

Additionally, the statistics for distance discrepancies in 66 non-repeated distances (among those 12 CPs), are presented in Fig. 16, for distances extracted from the G-TB LiDAR models, and in Fig. 17 for distances extracted from the G-VA models. The averaged distance statistics for all four users are shown on Fig. 18.

In Figs. 13, 14, 16, and 17, it is observed that user U24c attained lower discrepancies than the other 3 users. This could be attributed to the fact that user U24c has more experience in LiDAR modeling than the other ones, who were generating their first georeferenced point-cloud models in this project.

If the GCPs are preserved, the mentioned scanning procedures could be repeated and georeferenced in the same system. This will allow for the generation of point-cloud models at different time intervals for comparison and proper capture of displacement evolution along time.

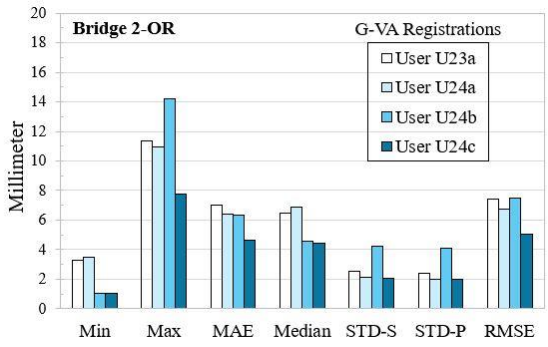

Fig. 14 4-user statistics of position discrepancies in 12 checkpoints – G-VA models vs RTS instrument

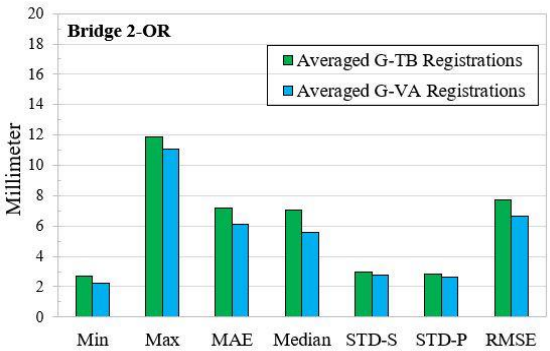

Fig. 15 4-user averaged statistics of position discrepancies in 12 checkpoints – LiDAR models vs RTS device

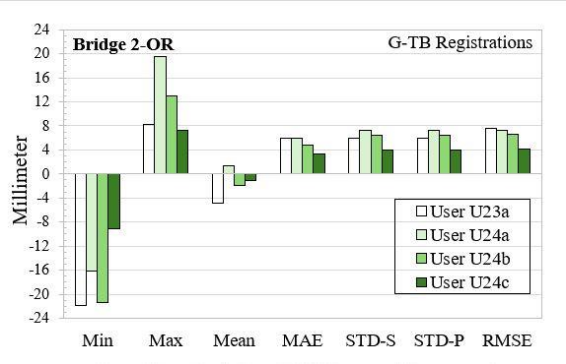

Fig. 16 4-user statistics of distance discrepancies in 66 non-repeated distances – G-TB models vs RTS device

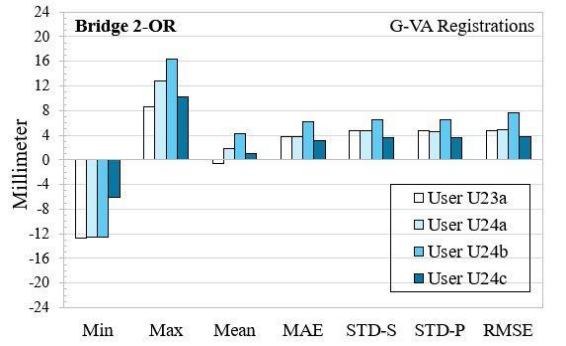

Fig. 17 4-user statistics of distance discrepancies in 66 non-repeated distances – G-VA models vs RTS

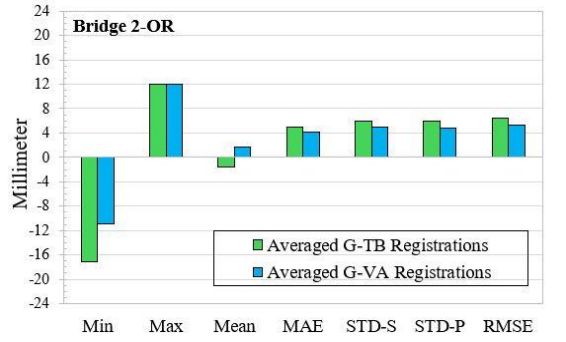

Fig. 18 4-user averaged statistics of distance discrepancies in 66 non-repeated distances – LiDAR models vs RTS

Also, it should be mentioned that the considered MSEWs were mostly covered by the main deck of the bridges. This facilitated the scanning procedures, even under rainy conditions. Additionally, laser scans do not need special lighting requirements, but the color components benefit from well-lit surfaces. Foggy weather may interfere with data acquisition.

5. Conclusions

This work compared the relative accuracy of LiDAR models with respect to measurements, completed in the field, with an accurate robotic total-station instrument. The main goal was to analyze the capacity of the resulting LiDAR models to potentially capture undesirable displacements in mechanically stabilized earth walls, acting as retaining walls at the abutments of two roadway bridges, 1-CG and 2-OR, in Georgia, USA. The analysis involved two different scan-stitching (registration) techniques. One is the target-based approach. It produces accurate LiDAR models, of any size, but requires longer times in the field to acquire several needed stitching targets for each scan. However, its associated postprocessing time, to generate final georeferenced LiDAR models, is relatively short, almost instantaneous if there were no errors. The other approach is Leica Geosystems' visual-aligned technique. In certain projects, with low scan superposition, the VA approach has been shown to be less accurate than the TB scheme. However, its main advantage is reduced time in the field. This is because it does not need to acquire 3 or more targets per scan. It only requires acquiring 3 or more targets, to georeference the whole final model (not for stitching each individual scan). The results obtained lead to the following conclusions and recommendations:

- Since the TB approach uses well materialized and accurately acquired fixed targets, it is expected to be more accurate than the VA one. However, as seen in this study, for relatively small areas (0.23 ha and 0.38 ha), with significant overlapping among all involved scans, the VA technique may become as accurate or even slightly better than the TB one. Nevertheless, a limitation of the current study is the fact that it does not determine the required minimum amount of overlapping for this to happen. However, analysis of the results from the three considered cases provides some guidance on this matter. The Herald Plaza case consisted of a rather large number of consecutive scans (34), covering a relatively large area (1.4 ha). The scans followed a closed loop around several contiguous buildings, where each scan showed overlapping with only a few previous and a few subsequent scans. The average separation between consecutive scanning stations was 14.9 m (ranging from 4.1 m to 26.8 m). Under these conditions, Fig. 6 shows that the VA approach was clearly less accurate (1.7 or 2 times less) than the TB scheme. However, when considering the smaller areas corresponding to bridges 1-CG (0.23 ha) and 2-OR (0.38 ha), where each was modeled with only 6 scans showing large superposition with their immediate neighbors, and also with all other scans, the VA technique was slightly more accurate than the TB approach, as seen in Table 10. In the case of the 1-CG bridge, its average scan separation was 24.5 m (ranging from 13.4 m to 42.9 m). For the 2-OR bridge, the average scan separation was 17.9 m (ranging from 14.0 m to 21.2 m).
- The VA approach is faster in the field than the TB one. This is because VA does not require each scan to acquire targets for stitching purposes. Only a few targets (a minimum of 3) are necessary for georeferencing the full model. On the other hand, the TB approach is slower in field operations, but faster while postprocessing data to register all scans.
- The resulting georeferenced registrations are to contain merged GCPs to attain improved accuracies. For this,

proper values are to be assigned to registration parameters in Leica's Cyclone Core software.

• As observed in Table 8, the LiDAR models of the MSEWs in bridge 1-CG were less accurate, in point positions, than those models for the MSEWs in bridge 2-OR. However, in distances, the models of 2-OR were slightly more accurate than those of 1-CG.

• Table 8 also shows that, for each of the two considered bridges, the resulting georeferenced LiDAR models, G-TB and G-VA, of their MSEWs, presented similar levels of discrepancies, in positions and in distances, with respect to measurements, performed in the field, via an accurate robotic, total-station instrument. That is, both approaches produced models with similar accuracies, and both could be employed at the same level of confidence to capture undesirable displacements of MSEWs. However, when using the VA approach scans are to show significant overlapping, as previously indicated.

• Regarding point positions, Table 9 shows that the LiDAR models of bridge 1-CG presents larger discrepancies (~2.0-2.8 times) with respect to the RTS device than the LiDAR models of bridge 2-OR. However, in distances, the discrepancies of the LiDAR models of bridge 1-CG present lower values (~0.6-0.8 times) than those of the LiDAR models of bridge 2-OR.

• Table 10 shows that, in both bridges, the G-VA models are slightly more accurate (~1.1-1.4 times in positions, and ~1.4-1.6 times in distances) than their G-TB models. This is ccontrary to what was observed in a previous study, the Herald Plaza project. The authors understand that the current reduced discrepancies in the G-VA models are since, in this project, each involved scan, out of 6 per bridge, presented substantial spatial superposition among all of them. That was not the case in the Herald Plaza project which required 34 consecutive scans, along a closed loop, with overlapped areas only between close neighboring ones. This emphasizes the need to attain proper scanning superposition when using the VA approach.

• In a root-mean-square sense, the results obtained from the point-cloud models in bridge 1-CG indicate that most MSEWs' displacements larger than, approximately, 24 mm could be captured by both LiDAR techniques, TB and VA.

• In a root-mean-square sense, the results attained from the point-cloud models in bridge 2-OR indicate that most MSEWs' displacements larger than, approximately, 11 mm could be captured by both LiDAR techniques, TB and VA.

• In bridge 2-OR, it was observed that LiDAR modelers, with previous training or experience, attained more accuracy, when extracting point positions and distances from their point-cloud models, than inexperienced ones. That is, previous training/experience reduced discrepancies by approximately 30%-50%. This experience factor may also contribute to the differences in accuracy observed in the first studied bridge, 1-CG, versus the second one, 2-OR.

• Since the noise level observed in both types of final models, G-TB and G-VA, is relatively low, and considering that an experienced team may capture most MSEWs' displacements larger than 11 mm (> ~½ inch), via the TB or VA approaches, both techniques are considered appropriate to monitor undesirable displacements of MSEWs. The user may select one or the other scheme, depending on where they prefer to spend more or less time in the field, acquiring data, or at a computer laboratory postprocessing it.

• The scanning frequency for routine inspections has not been determined by this study. The two bridges considered have been visited and modeled twice in a one-year interval, using the same GCPs, but no wall displacements were found. Communications with experienced contractors indicated that displacements and settlements in MSEWs are more likely to occur during and just after construction. Witnesses have observed displacements of ~15 cm. Nevertheless, the authors estimate that an annual inspection is appropriate. Additionally, after a major weather event (hurricane, flood, etc.) inspections should be carried out.

The authors plan to expand this study to incorporate the comparison of not just a few CPs, but full point clouds generated by both analyzed approaches, TB and VA, at different times, for monitoring potential displacements at MSEWs in Georgia bridges.

Acknowledgments

The authors express their gratitude for the support, assistance, and dedication provided by GDOT personnel, while facilitating the completion of this project. Nevertheless, the contents and views expressed in this article are solely those of the authors and do not reflect the opinions of GDOT or its representatives.

Numerous hardworking undergraduate and graduate students actively participated in this work. They were either attending Senior Project or Intro to Terrestrial LiDAR courses. They are Tanvir Ahmed, David Anderson, David Arteaga, Oliver Arteaga, Jakeb Britt, Turvon Casey, Olivia Duffy, Blake Forbes, Ralph Franks, Jabari Greene, Evan Hall, Noah Hallman, Iffat Haq, Reece Hart, Chase Hovis, Syed Hussan, William Immel, Kobe Keise, Garyn King, Charles Lawal, Amber Lawrence, William Loyed, Andrew Musmanno, Jacob Reaves, Riyadul Riyad, Joshua Rogers, Chase Simington, Zachary Swindell, Jerry Thomas, Garfield Thorpe, Aniya Williams, Jared Worthy, and Chandler Yarbrough.

References

Becker, D., Raddatz, L., Roussel, C. and Klonowski, J. (2024), "Analysis methods for deformation detection using TLS and UAS data on the example of a landslide simulation", *Int. J. Geo-Eng.*, **15**, 9. https://doi.org/10.1186/s40703-023-00203-z.

Berg, R.R., Christopher, B.R. and Samtani, N.C. (2009a), "Design and Construction of Mechanically Stabilized Earth Walls and Reinforced Soil Slopes – Volume I", *Federal Highway Administration, Department of Transportation*, Washington D.C. https://rosap.ntl.bts.gov/view/dot/49730/dot_49730_DS1.pdf.

Berg, R.R., Christopher, B.R. and Samtani, N.C. (2009b), "Design

and construction of mechanically stabilized earth walls and reinforced soil slopes – Volume II", *Federal Highway Administration, Department of Transportation*, Washington D.C. https://highways.dot.gov/sites/fhwa.dot.gov/files/FHWA-NHI-10-025.pdf.

Federal Highway Administration, Department of Transportation, USA (2022), "National Bridge Inspection Standards", *National Archives and Records, Federal Register*, **87**(88). https://rosap.ntl.bts.gov/view/dot/77619/dot_77619_DS1.pdf

Jensen, W. (2009), "Inspector's manual for mechanically stabilized earth walls", *Nebraska Department of Roads*, Nebraska Transportation Center, Report No. SPR-P1(09) P320. Available at the below link, accessed on December 6, 2024. https://digitalcommons.unl.edu/cgi/viewcontent.cgi?article=1013&context=matcreports.

Ko, Y., Seo, S., Jin, T. and Chung, M. (2021), "Feasibility evaluation of the 3D-DIC noncontact measurement system using small-scaled model test of earth retaining wall", *Int. J. Geo-Eng.*, **12**, 12. https://doi.org/10.1186/s40703-021-00141-8.

Leica Geosystems (2007), "Leica TPS1200+ Series Technical Data", 16 pages. https://hts-3d.com/brochures/Leica-TS1201-Total-Station.pdf.

Leica Geosystems (2014), "Leica ScanStation C10 The All-in-One Laser Scanner for Any Application", 2 pages. https://www.universityofgalway.ie/media/publicsub-sites/engineering/files/Leica_ScanStation_C10_DS.pdf.

Lim, H., Park, J., Kim, J. and Ko, J. (2023), "Numerical study on stability and deformation of retaining wall according to groundwater drawdown", *Geomech. Eng.*, **33**(2), 195-202. https://doi.org/10.12989/gae.2023.33.2.195.

Loosli, E. (2025), "LiDAR vs. photogrammetry: what sensor to choose for a given application", https://wingtra.com/lidar-drone/lidar-vs-photogrammetry-what-sensor-to-choose/. February 13, 2025.

Maldonado, G.M., Maghiar, M. and Loyed, W.A. (2024), "Spatial and distance discrepancies in target-based and visual-aligned LiDAR models", *Proceedings of the ASC 2024 60th Annual ASC International Conference*, *Epic Series in Built Environment*, **5**, 505-513. https://doi.org/10.29007/wd8k.

Mitchell, J.K. and Villet, W.C.B. (1987), "Reinforcement of earth slopes and embankments", *National Cooperative Highway Research Program*, Washington D.C. http://onlinepubs.trb.org/onlinepubs/nchrp/nchrp_rpt_290.pdf.

Sun, C. and Graves, C. (2013), "Evaluation of mechanically stabilized earth walls for bridge ends in Kentucky; What Next?", *University of Kentucky, Kentucky Transportation Center*, Report No. KTC-13-11/SPR443-12-1F. http://dx.doi.org/10.13023/KTC.RR.2013.11.

Tarawneh, B. and Siddiqi, J. (2014), "Performance issues of mechanically stabilized earth wall supporting bridge abutment", *Proceeding of the 8th International Conference on Engineering and Technology Research*, Dubai, United Arab Emirates. https://doi.org/10.13140/RG.2.2.20272.66560.

Transportation Research Board (2012), "Assessing the long-term performance of mechanically stabilized earth walls", *The National Academies Press*, Washington, DC. https://doi.org/10.17226/22721.

Vankavelarr, D.P. and Leshchinsky, D. (2002), "Inspection guidelines for construction and post-construction of mechanically stabilized earth wall", *Delaware Center for Transportation, University of Delaware*. https://bpb-us-w2.wpmucdn.com/sites.udel.edu/dist/1/1139/files/2013/10/Rpt.-143-Mechanically-Stabilized-Earth-Wall-Final-Leshchinsky-yxyg38.pdf.

Wang, J., Li, W., Rui, R., Zhai, Y. and He, Q. (2023), "Experimental investigation of earth pressure on retaining wall and ground settlement subjected to tunneling in confined space", *Geomech. Eng.*, **32**(2), 179-191. https://doi.org/10.12989/gae.2023.32.2.179.

Wisconsin DOT (2017), "WisDOT Structure Inspection Manual, Part 4 – Ancillary Structures", *Wisconsin DOT*. https://wisconsindot.gov/dtsdManuals/strct/inspection/insp-fm-pt4ch4.pdf.

IC